How Natural Convection Can Cancel Heating by Piston Effect[1]

A. Jounet[2,4] , S. Amiroudine[3], A. Mojtabi[2], B. Zappoli[3]

[1] Paper presented at the Thirteenth Symposium on Thermophysical Properties, June 22-27, 1997, Boulder, Colorado, U.S.A.

[2] Institut de Mécanique des Fluides de Toulouse, UMR CNRS/INP-UPS 5502, UFR MIG, Université Paul Sabatier, 118, route de Narbonne, 31062 Toulouse Cédex, France.

[3] Centre National d'Etudes Spatiales, 18, Av. E. Belin, 31405 Toulouse Cédex 04, France.

[4] Corresponding author.

ABSTRACT

This work aims to bring some new insights to the question of Piston Effect heat transfer, which has been found to be the main cause of temperature equilibration in the vicinity of the liquid-vapor critical point under weightlessness conditions. The thermalization process of a near-critical fluid confined in a cavity and submitted to local heating is analyzed with special emphasis on the role of gravity and boundary conditions. The solution of the unsteady Navier-Stokes equations written for a hypercompressible low-heat-diffusing van der Waals gas is obtained in the 2-D configuration by means of a finite-volume numerical code. Under earth gravity conditions, the results show that the thermal plume rising from a thermistor strongly decreases and rapidly cancels bulk fluid heating when it strikes the top thermostated wall. It is proved that heat transfer by Piston Effect is not prevented by convection, but that the sudden enhancement of the cooling Piston Effect generated at the thermostated top boundary leads to an early equilibrium between the cooling and heating Piston Effects.

KEY WORDS: acoustic waves; convection; diffusion; heat transfer; near-critical fluid; piston effect.

1. INTRODUCTION

It has recently been found that the fast temperature equilibration occurring in near critical fluids under conditions of weightlessness is achieved by a new heat transfer process named the Piston Effect (PE). In fact, when a confined near-critical fluid is heated at its boundaries, the fluid contained in the thin thermal adaptation layer expands strongly because of its diverging compressibility. This expansion adiabatically compresses the rest of the fluid and causes a homogeneous increase of the temperature. In contrast with pure diffusion, this thermoacoustic heat transfer mechanism becomes increasingly efficient as the critical point is approached, and the thermal equilibration time becomes shorter. First theoretically predicted by different teams in 1990 [1,2,3], the PE has been extensively explored in several analytical [4,5,6] , numerical [7,8] and experimental [9,10] studies.

Despite the high hydrodynamic instability observed on the ground in near-critical fluids, it has been recently shown that the PE is still present under one-*g* conditions [8]. Indeed, even if the temperature is almost homogeneous in the whole fluid due to the PE, a very small temperature inhomogeneity causes a large density inhomogeneity in such a hypercompressible fluid. Thus, the steep density gradients that appear in the thermal boundary layer trigger a strong flow in a quasi-isothermal fluid. Nevertheless, recent experiments performed on earth [11] have shown that the near-critical fluid heated by an immersed thermistor in a non-insulated cell undergoes almost no warming compared with that observed under microgravity conditions. In the present study, we reproduced the conditions described above in our simulation code to analyze the physical processes occurring. The influences of the thermal boundary conditions and of convection are clearly established. In particular, it is shown that when the hot convective plume rising from the thermistor strikes the thermostated upper wall, the cooling PE generated at this boundary is strongly enhanced, thus drastically slowing down the homogeneous heating of the bulk phase. Then, the cooling and heating PE quickly balance each other as the cold boundary layer (CBL) becomes entirely immersed by the flow, and the bulk fluid temperature stops increasing.

The model and the governing equations are presented in §2, the numerical method in §3 while §4 is dedicated to the results and discussion.

2. THE MODEL AND GOVERNING EQUATIONS

The model used to simulate the behaviour of the supercritical fluid is the same as the one already used in Refs. [4,5,8]. We basically consider a 2-D square cavity filled with near critical CO_2 submitted to gravity. The heating source, located at the center of the domain, provides constant power while all the boundaries are adiabatic, except the top wall which is maintained at constant temperature (Fig. 1). The fluid is initially at rest, stratified in density and at thermal equilibrium.

The non-dimensional variables (density, temperature, pressure, velocity, space and time) introduced in the conservation equations are defined as:

$$\rho = \frac{\rho'}{\rho'_c};\ T = \frac{T'}{T'_c};\ \ P = \frac{P'}{\rho'_c R' T'_c};\ \vec{v} = \frac{\vec{v}'}{c'_0};\ \vec{x} = \frac{\vec{x}'}{L'};\ t = \frac{t'}{t'_a}$$

where ρ'_c and T'_c are the critical coordinates (467.8 kg/m^3 and 304.13 K, respectively), R' the specific perfect gas constant, $c'_0 = \sqrt{\gamma_0 R' T'_c}$ the sound velocity for the perfect gas in which γ_0 is the specific heats ratio (for the perfect gas), L' the length of the cavity (10 mm), and $t'_a = L'/c'_0$ a characteristic acoustic time.

The thermistor is simulated by means of local power injection inserted in the energy equation by the non-dimensional term: r. $r = r'/r'_0$, with $r'_0 = \rho'_c R' T'_c c'_0 / L'(\gamma_0 - 1)$ and $r' = \dot{Q}'_l / S'_Q$ where $\dot{Q}'_l$ represents the heating rate per unit length (0.74 W.m^{-1} in our basic case) and S'_Q the section of the wire representing the thermistor.

Concerning the model of the critical behaviour, beside the van der Waals equation of state which exhibits a $(T' - T'_c)^{-1}$ divergence of compressibility, the following law is considered to take the thermal conductivity divergence into account: $\lambda = \lambda'/\lambda'_0 = 1 + 0.75\left((T' - T'_c)/T'_c\right)^{-1/2}$. Both these equations were chosen with a concern for simplicity. Even though they do not lead to the correct critical exponents, they permit rich phenomenological investigations which have already provided some very

relevant qualitative information on the processes occurring in near-critical fluids. More information concerning this choice can be found in previous studies [4, 5, 6, 8].

Then, the resulting system of equations is:

$$\frac{\partial \rho}{\partial t} + \quad (\rho \vec{v}) = 0 \tag{1}$$

$$\frac{\partial (\rho \vec{v})}{\partial t} + \quad (\rho \vec{v} \quad \vec{v}) = -\gamma_0^{-1} \quad P + \varepsilon[\quad {}^2\vec{v} + \frac{1}{3} \quad (\quad \vec{v})] + \frac{1}{Fr_0} \rho \vec{g} \tag{2}$$

$$\begin{aligned} \frac{\partial (\rho T)}{\partial t} + \quad (\rho \vec{v} T) &= -(\gamma_0 - 1)(P + \frac{9}{8}\rho^2)(\quad \vec{v}) \\ &+ \frac{\varepsilon \gamma_0}{\mathrm{Pr}_0} \quad [(1 + 0.75(T-1)^{-05}) \quad T] \\ &+ \varepsilon \gamma_0 (\gamma_0 - 1)(v_{i,j} v_{j,i} + v_{i,j} v_{i,j} - \frac{2}{3} v_{i,i} v_{j,j}) + r \end{aligned} \tag{3}$$

$$P = \frac{\rho T}{1 - 1/3\rho} - \frac{9}{8}\rho^2 \tag{4}$$

where $\mathrm{Pr}_0 = \nu_0^{'} / \chi_0^{'}$ represents the Prandtl number ($\nu_0^{'}$ and $\chi_0^{'}$ are the reference kinematic viscosity and thermal diffusivity, respectively, at critical density for an ideal gas), $Fr_0 = c_0^{'2} / L^{'} g_0^{'}$ is the Froude number with $g_0^{'}$=9.8m.s^{-2}, and $\varepsilon = \mathrm{Pr}_0 \, t_a^{'} / t_d^{'}$ $(t_d^{'} = L^{'2} / \chi_0^{'})$.

In the vicinity of the critical point (CP), the initial conditions can be written as:

$$\vec{v} = 0; \;\; T = 1 + \mu; \; \rho(y) = \exp(-K(y-1)); \; P(y) = \frac{3}{2}(1+\mu) - \frac{9}{8} + \frac{9}{4}\mu \exp(-K(y-1))$$

with: $\mu = (T_i^{'} - T_c^{'}) / T_c^{'}$ ($T_i^{'}$ the initial temperature, taken 1K warmer than $T_c^{'}$ in our calculations) and $K = 4 g \gamma_0 / 9 \mu Fr_0$ (g is the non-dimensional gravity level).

At the boundaries, the conditions are: $\vec{v} = 0$; $T(y=1) = 1 + \mu$; $\partial T / \partial n \, (y \neq 1) = 0$.

In this study, we are not interested in the description of acoustic waves and since the flow Mach number is very low, the pressure is split into two parts and the equations are re-scaled with a longer reference time (acoustic filtering method, see [12]). Thus, one chooses the PE time scale [4,5], which is smaller than the convection time scale: $\tau = t \, \varepsilon / \mu^{3/2}$, while the corresponding reference velocity is given by: $U^{'} = c_0^{'} \, \varepsilon / \mu^{3/2}$.

3. NUMERICAL METHOD

The numerical method adopted in our code is the finite-volume method, using a staggered grid in order to avoid pressure oscillations [13]. The SIMPLER algorithm [13] was used to perform the resolution. At the discretization stage, a Power Law scheme was used in the model. Because of the question of the influence that the artificial viscosity might have on the results [14], the calculations were also tested with a QUICK scheme [15], without great changes being exhibited.

Concerning the mesh frame, it was refined in the thermal boundary layer regions, *i.e.* at the center of the cell and close to the top wall, by means of a power law series. But since the flow was found to be rather turbulent in the presence of gravity, the grid must also be thin over the whole domain. Such constraints led us to choose a 200*200 point mesh with a 1.6 boundary refining exponent and a resulting 5.10^{-3} non-dimensional time step.

4. RESULTS AND DISCUSSION

4.5 Flow Pattern

Because of the large compressibility and very low diffusivity of the fluid, steep density gradients (about 5.10^4 kg/m^4) appear close to the heat source, which is only 2K warmer than the initial temperature. Consequently, the buoyancy force generates an intense flow (velocity reaches 15 mm/s) which looks like a plume rising to the top wall (Figs. 2, 3, 4 & 5). The temperature of the convected fluid rapidly decreases. Only the small portion of fluid located in the core part of the plume is significantly warmer than the rest of the fluid, and neither convection nor diffusion carries away a lot of heat. Thus, the PE remains the main cause of bulk heating. It must be reported that a cooling PE (CPE) appears because of the thermostated wall: a very thin thermal adaptative layer (the CBL) forms in which the hypercompressible fluid strongly contracts due to the cooling imposed by the wall and in turn generates a regime of expansion acoustic waves causing homogeneous cooling of the fluid. Therefore, the PE results from the

competition between the heating PE (HPE) produced by the fluid heated by the thermistor and the CPE.

After less than 1 s, the upward plume strikes the top wall and is spread along it in a quasi-turbulent way. Indeed, in addition to both rotative cells formed by viscous coupling, the cooler fluid located in the CBL tends to flow down, like drips, while the fluid convected in the plume is still buoyant. Some recirculation flows appear on either side of the stagnation point area and the CBL structure is greatly modified. Two essential steps occur during the CBL structural changes, the consequences of which on cavity thermalization are discussed in the next section. First around τ=3.5 (0.8 s), when the rising flow begins to strike the middle of the top wall. The temperature elevation profile at this moment is plotted in Fig. 6. It can be observed that the gradients suddenly increase in the CBL due to convection which reduces the diffusion layer thickness and, at the same time, makes the outer temperature of the CBL warmer. Likewise, at τ=9, sudden temperature gradient increases occur on both corners of the CBL (Fig. 7): a warmer quasi-bubble becomes separated from the vortex flows because of the buoyancy and strikes both sides of the isothermal wall.

4.2 Fluid Thermalization

The temperature variations caused by the PE, measured at a point of the cavity where neither convection nor diffusion brings any heat, are plotted versus time on Fig. 8. After a continuous increase, two inflection points appear around τ=3.5 and τ=9 (2.1 s) which then lead to an almost constant value (28 mK). This early end to heating by PE contrasts with what happens at g=0, the temperature elevation of which is plotted in Fig. 9, curve 2 (curve 1 represents the plot of Fig. 8), and which exhibits a continuous increase. In curves 3 and 4 of Fig. 9 all the walls are insulated in the presence (3) or absence (4) of gravity. They show that HPE is only little disturbed by convection, as already observed in another configuration [8], and prove that the end to heating observed in Fig. 8 is necessarily linked with some modifications of the CPE. These curves also show that the fluid heating rate by the PE (constant) is proportional to the

injected heat flux, a result which is consistent with previous analytical works and even quantitatively fits some theoretical results [5,6]. Similarly, the inflection points appearing in Fig. 8 exactly correspond to those of the total heat flux lost at the thermostated wall, and the heating by PE stops when the evacuated heat flux equals the power injected by the thermistor (Fig. 10). The local CBL thermal gradient increases pointed out in the previous section at τ=3.5 and τ=9 correspond to sudden convection-driven diffusion. In turn, these local enhancements of the fluid cooling in the CBL generate stronger CPEs. Therefore, the inflections in fluid heating correspond to local and sudden CPE enhancements. From τ=10 (2.38 s), the CPE gets strong enough to balance the HPE. Then, since no major changes affect the CBL thermal structure despite the very transient nature of the flow, bulk heating by the PE stops. The almost total absence of heating over long periods observed experimentally in a near-critical fluid thus seems to result from the cancelling of the two antagonistic PEs, which is accelerated by convection near the CBL.

Conclusion

The mechanism of temperature equilibration in a near-critical pure fluid under earth gravity conditions has been identified by means of numerical simulations. Some new insights into the question of the interplay between convection and the Piston Effect have been gained. In particular, it has been found that far from being due to the cancelling of the Piston Effect by convection, the absence of Piston Effect heating results from Cooling Piston Effect enhancement which occurs when the temperature field is locally modified by convection close to the thermostated boundary. An early balance between the Heating Piston Effect and the Cooling Piston Effect can then appear which stops any overall Piston Effect heating.

REFERENCES

[1] B. Zappoli, D. Bailly, Y. Garrabos, B. Le Neindre, P. Guenoun & D. Beysens, *Phys. Rev. A*, 41, 2264 (1990).

[2] H. Boukari, J.N. Shaumeyer, M.E. Briggs, R.W. Gammon, *Phys. Rev. A*, 41 (1990).

[3] A. Onuki, H. Hao & R.A. Ferrel, *Phys. Rev. A*, 41, 2256 (1990).

[4] B. Zappoli, *Phys. Fluids A*, 4, 1040 (1992).

[5] B. Zappoli & P. Carlès, *Eur. J. Mech. B*, 14, 1, 41 (1995).

[6] P. Carlès, *Ph. D. Dissertation* (1995).

[7] B. Zappoli & A. Durand-Daubin, *Phys. Fluids*, 6, 1929 (1994).

[8] B. Zappoli, S. Amiroudine, P. Carlès & J. Ouazzani, *J. Fluid Mech.*, 316, 53 (1996).

[9] P. Guenoun, D. Beysens, B. Khalil, Y. Garrabos, B. Kammoun, B. Le Neindre & B. Zappoli, *Phys. Rev. E*, 47, 1531 (1993).

[10] M. Bonetti, F. Perrot, D. Beysens & Y. Garrabos, *Phys. Rev. E*, 49 (1994).

[11] D. Beysens, *private communication* (1995).

[12] S. Paolucci, *SAND*, 82-8257 (1982).

[13] S.V. Patankar, Numerical heat transfer and fluid flow, *Hemisphere*, (1980).

[14] B.P. Leonard & J.E. Drummond, *Int. J. Num. Methods Fluids*, 20, 421 (1995).

[15] T. Hayase, J.A.C. Humphrey & R. Greif, *J. Comput. Phys.*, 98, 108 (1992).

FIGURE CAPTION

Fig. 1. The center heated 2-D square cavity.

Fig. 2. Thermal field at τ=2.

Fig. 3. Thermal field at τ=5.

Fig. 4. Thermal field at τ=10.

Fig. 5. Velocity field at τ=10.

Fig. 6. Temperature elevation profiles close to the CBL at the time of the first shock of the plume: τ=3.2 (curve 1), τ=3.4 (2), τ=3.6 (3) and τ=3.8 (4).

Fig. 7. Thermal field close to the CBL at τ=9.2.

Fig. 8. Temperature variations in the bulk fluid versus time.

Fig. 9. Comparison of the PE heating for g=1 (curves 1 and 3) or g=0 (curves 2 and 4), with the upper wall being either thermostated (curves 1 and 2) or adiabatic (curves 3 and 4).

Fig. 10. Heat fluxes injected by the thermistor (curve 1) and lost at the non-insulated boundary (curve 2) versus time.

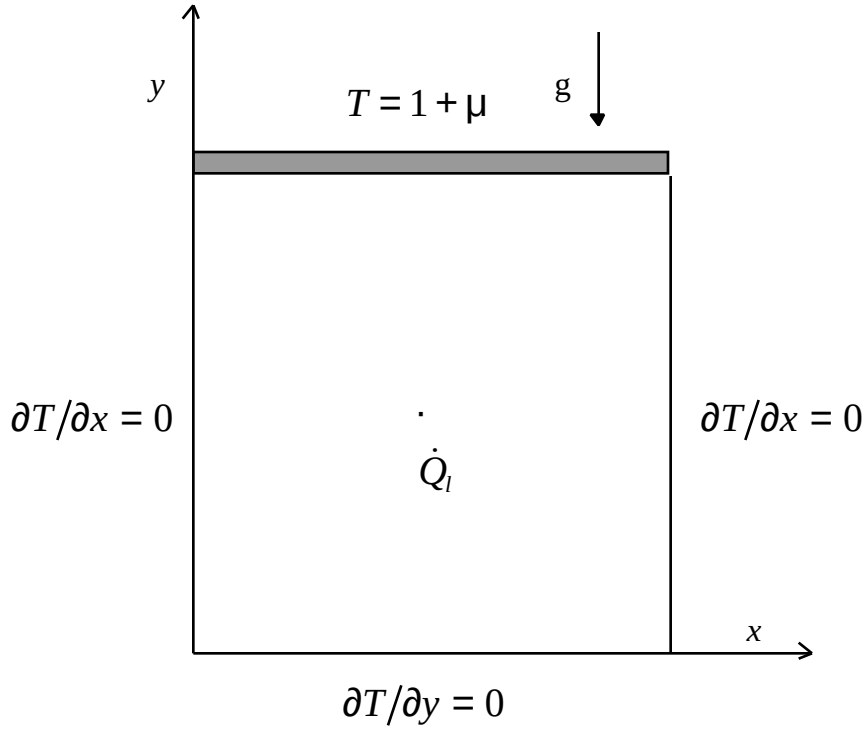

Fig. 1.

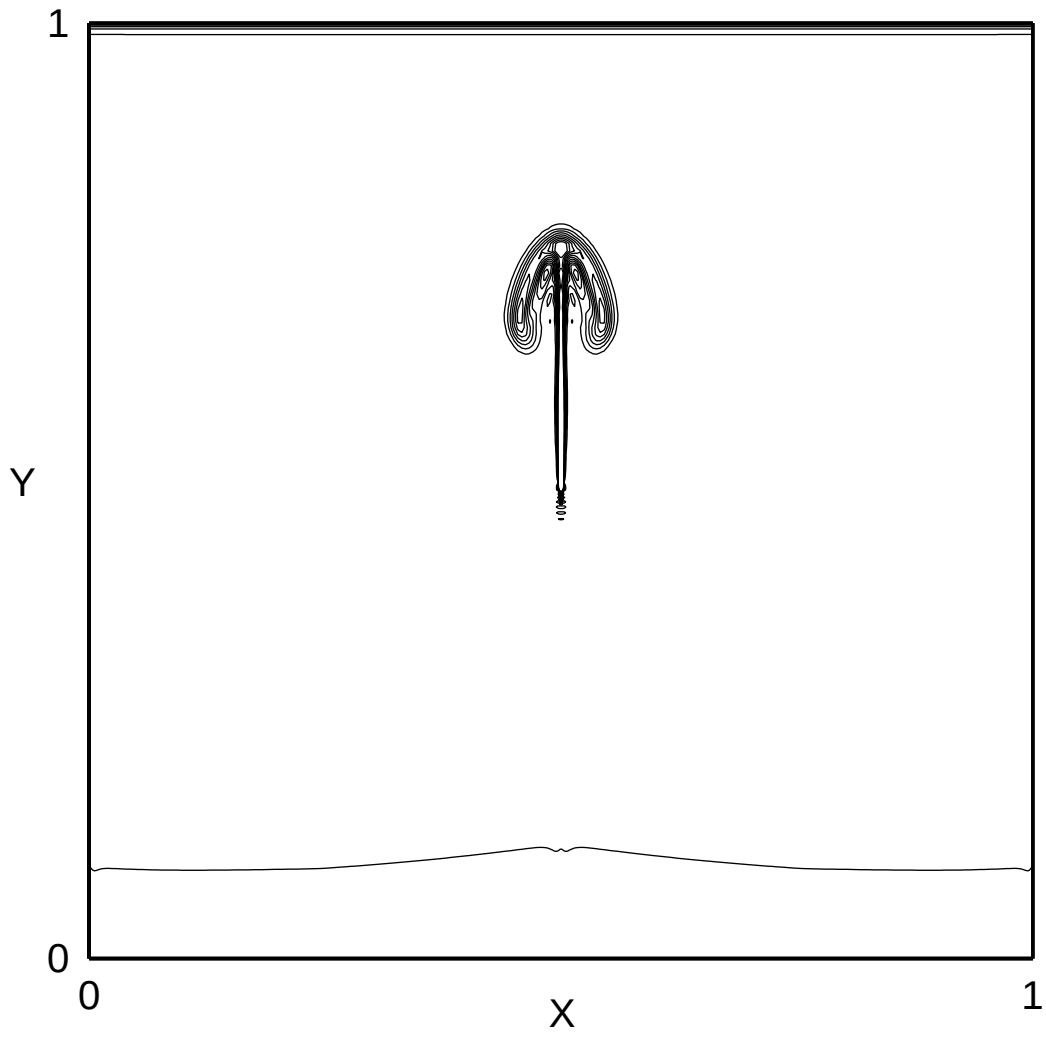

Fig. 2

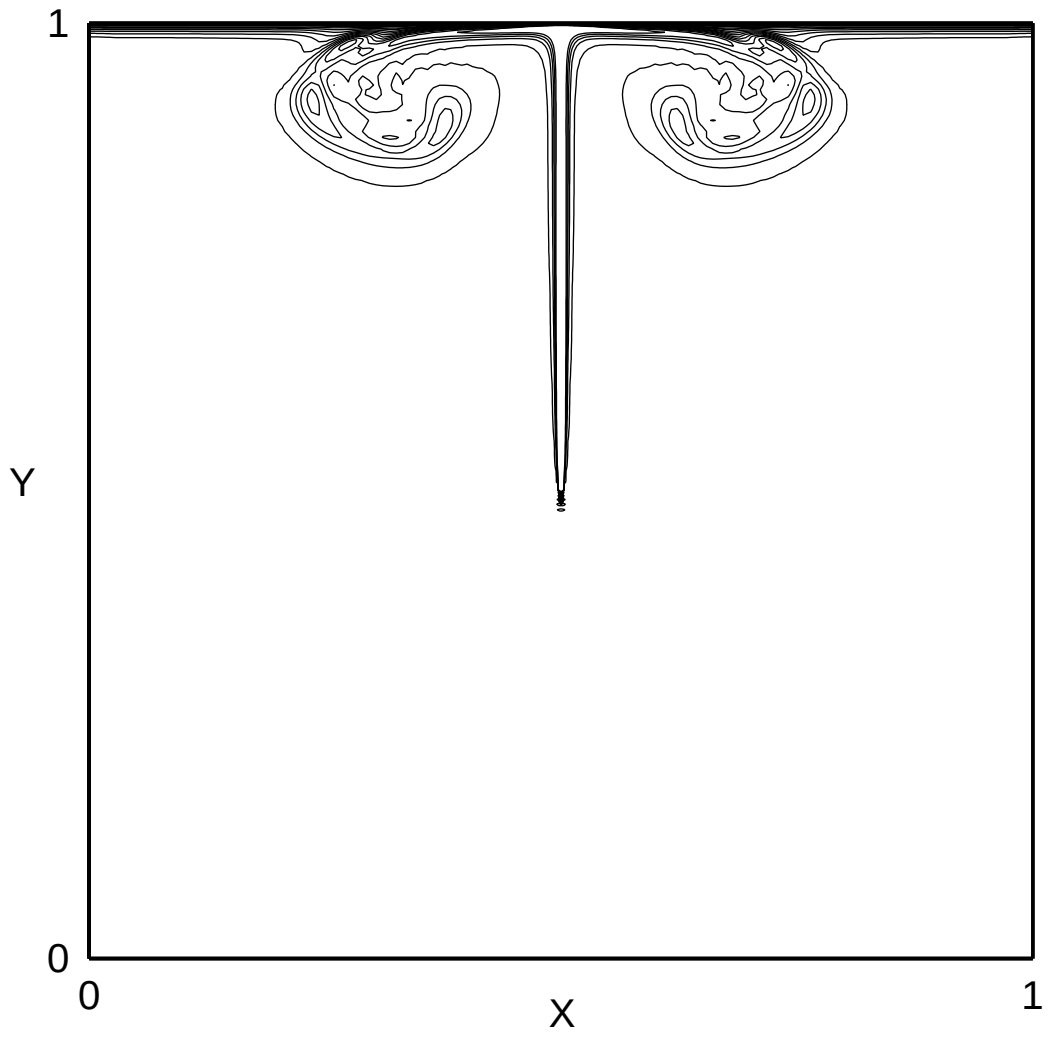

Fig. 3

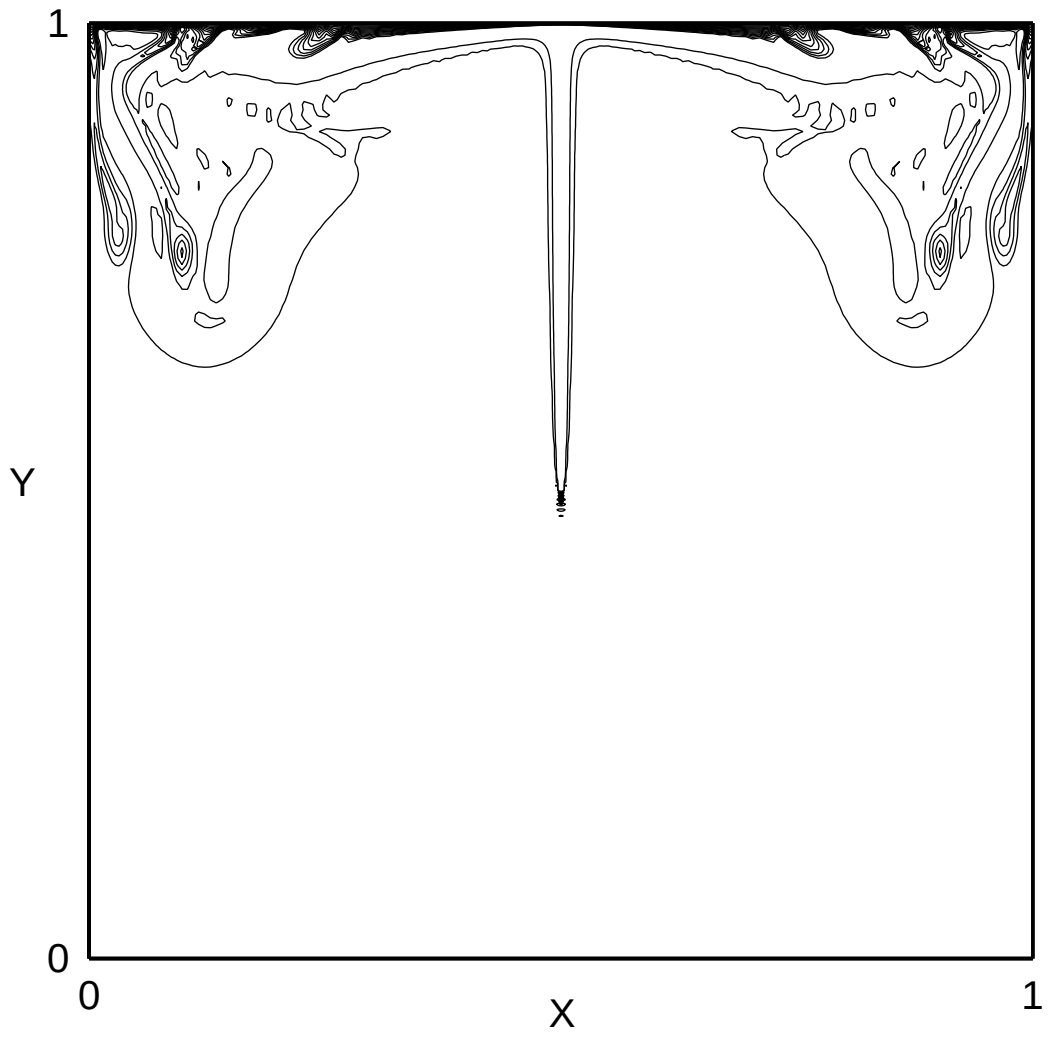

Fig. 4

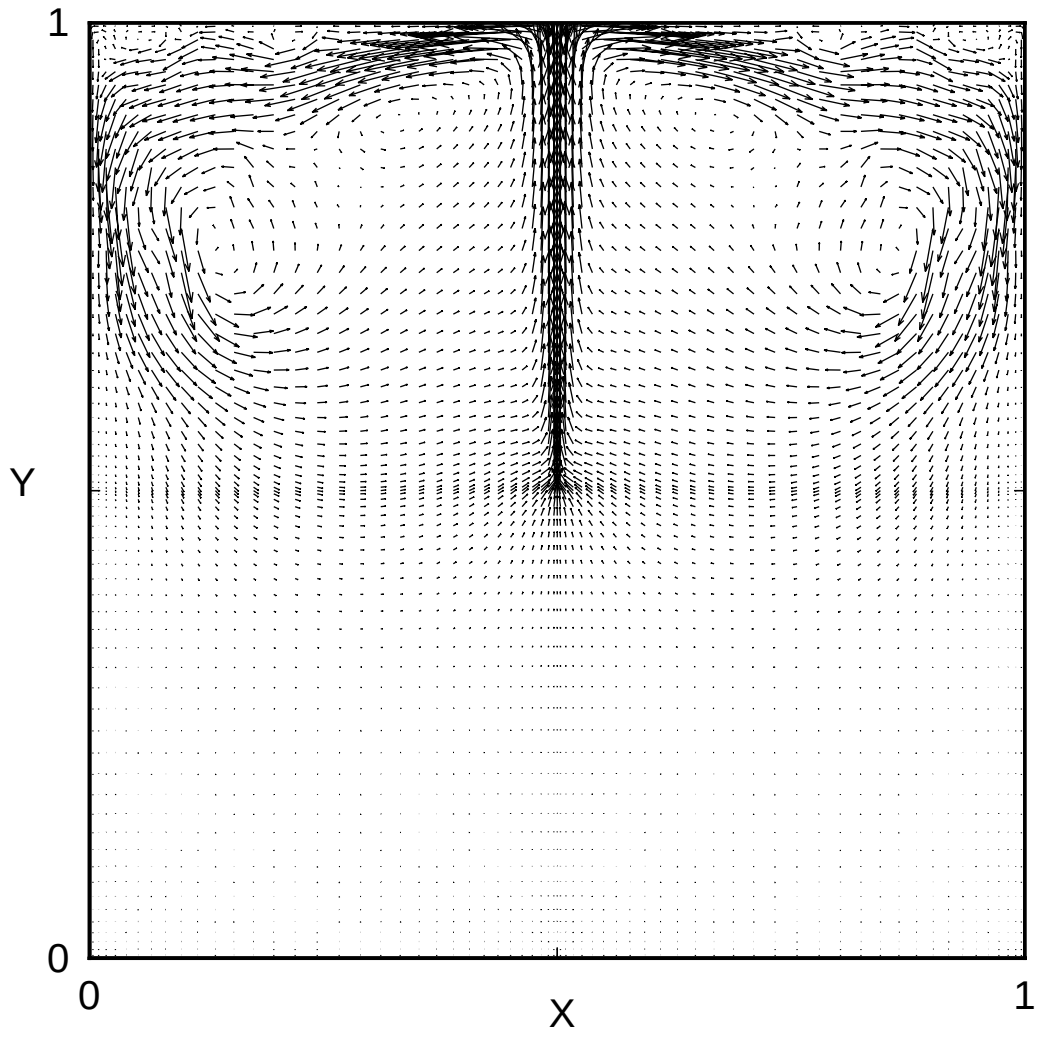

Fig. 5

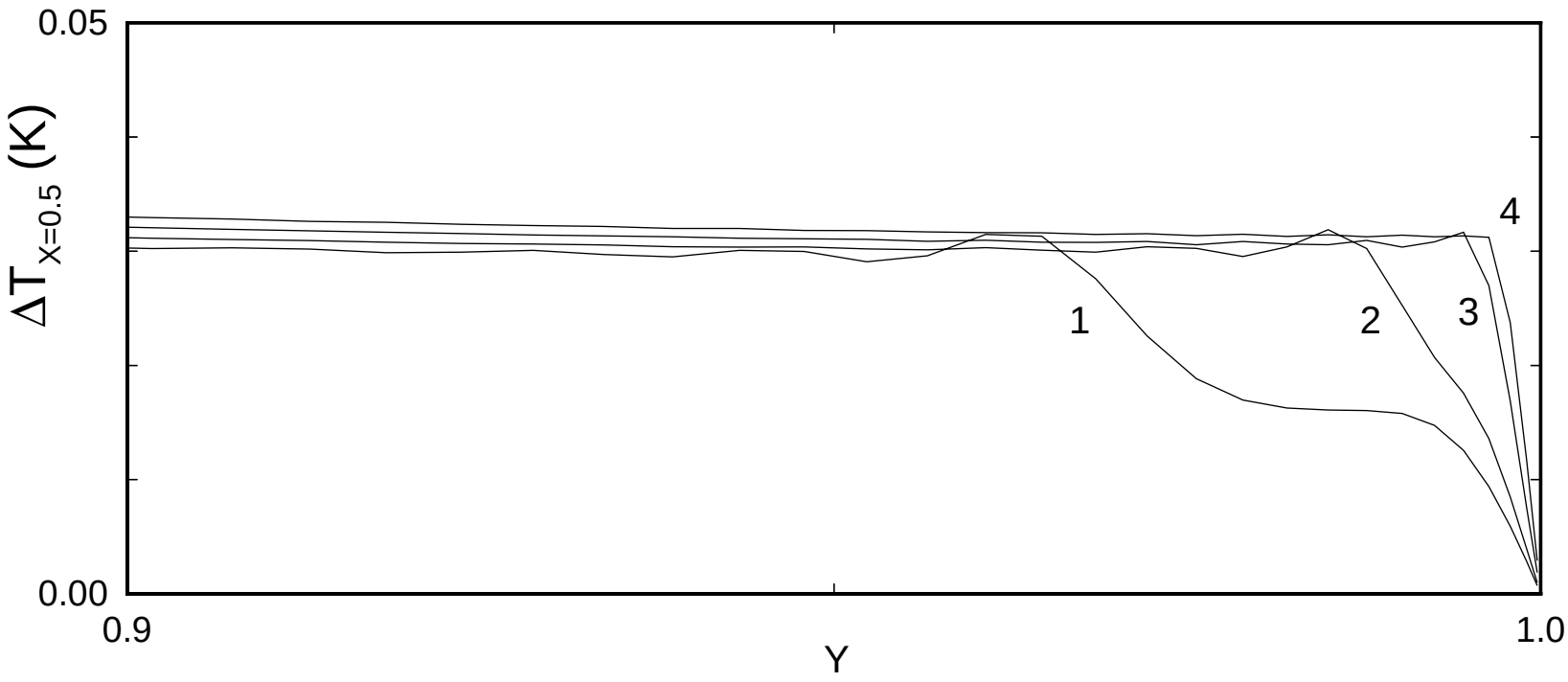

Fig. 6

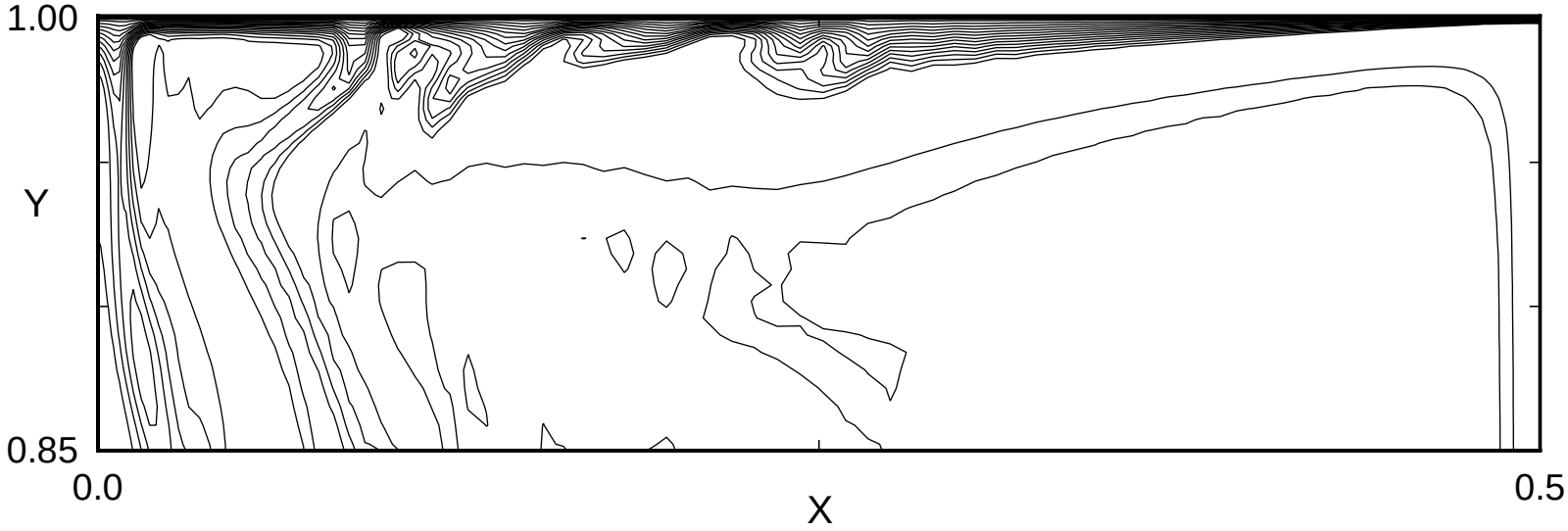

Fig. 7

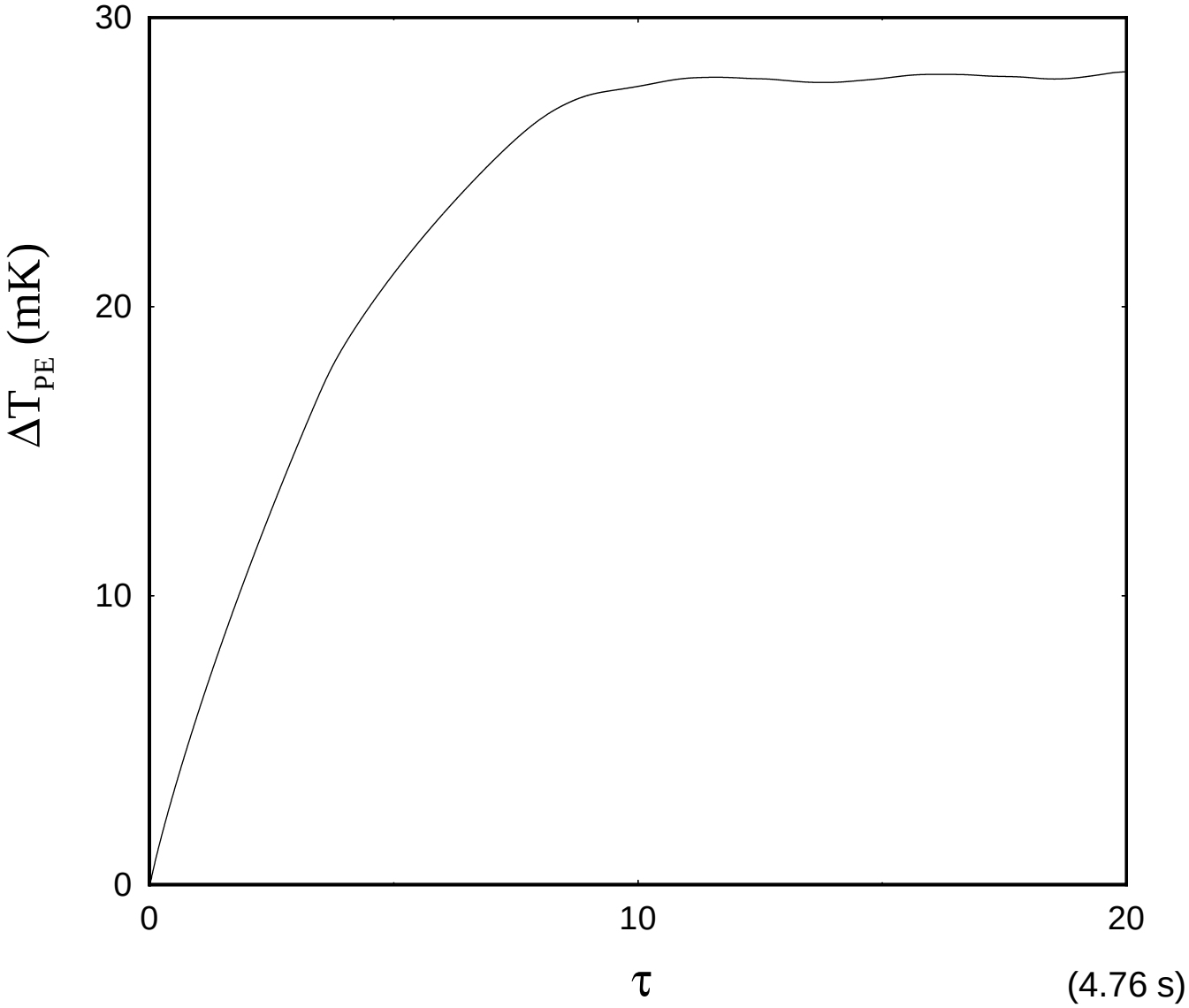

Fig. 8

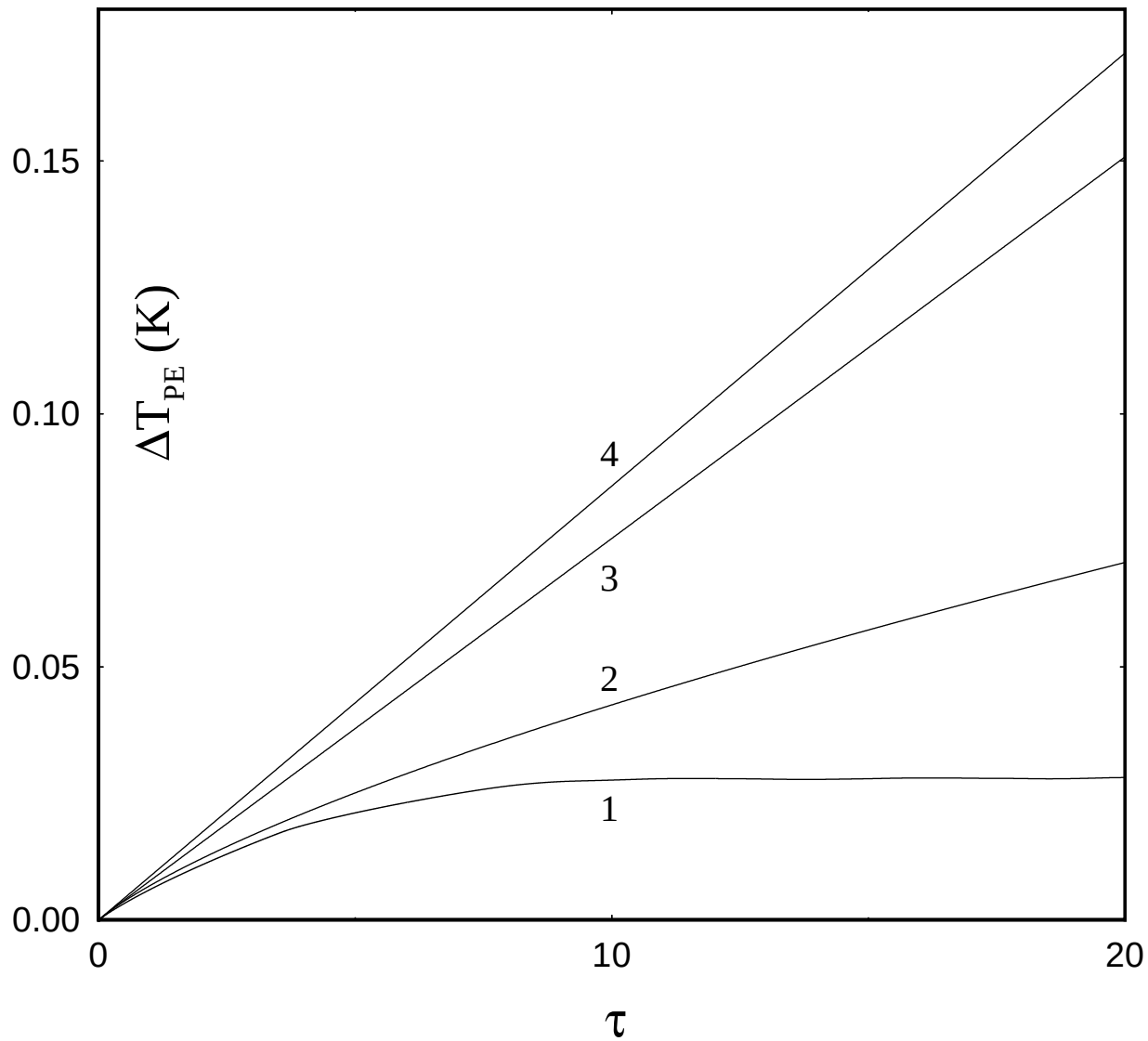

Fig. 9

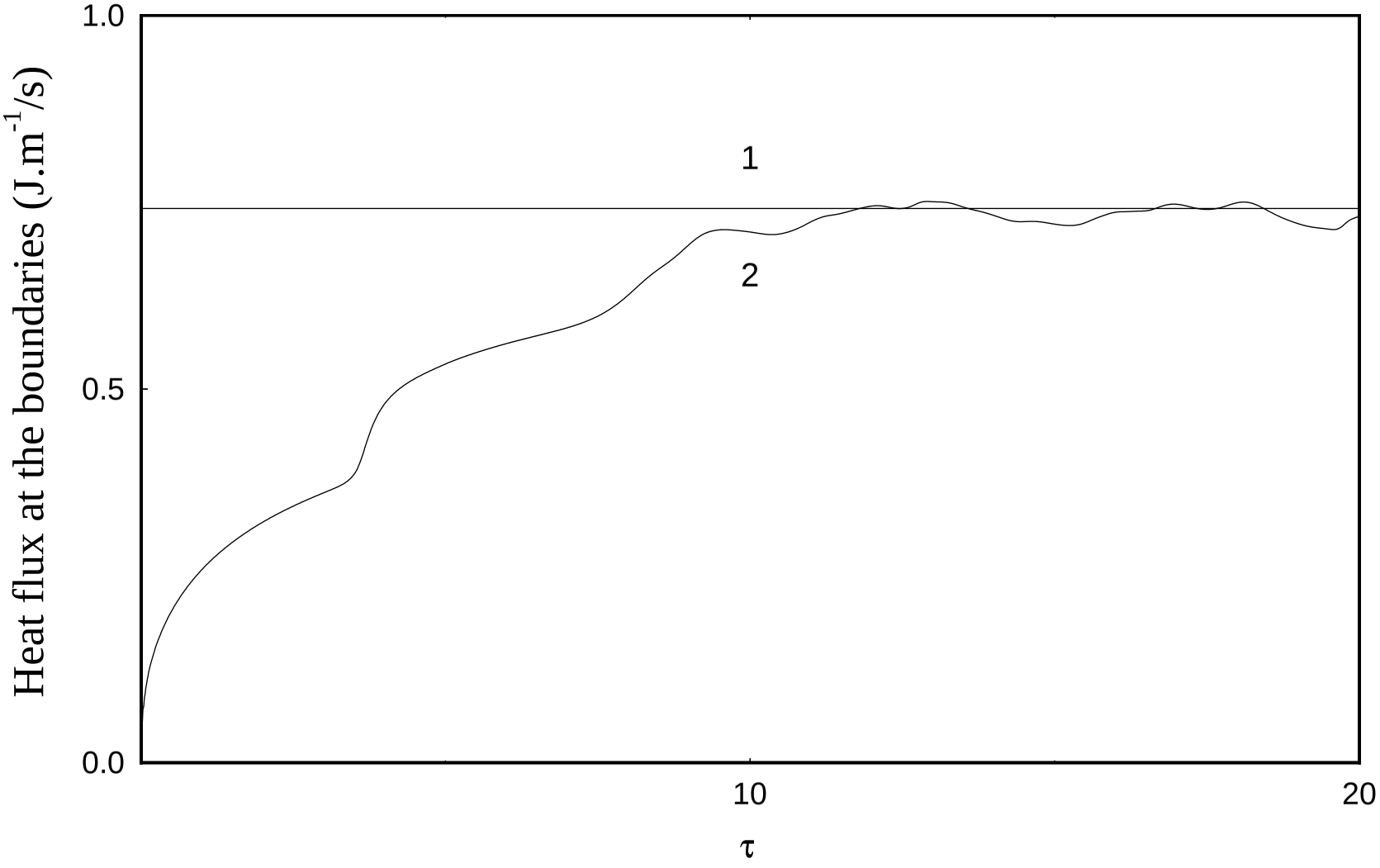

Fig. 10